Automated tool for nuclei detection in digital microscopic images: Application to retinal images

Jiyun Byun [a,b], Mark R. Verardo [b,c], Baris Sumengen [a,b], Geoffrey P. Lewis [b,c], B. S. Manjunath [a,b] and Steven K. Fisher [b,c,d]

[a]Department of Electrical and Computer Engineering
[b]Center for Bioimage Informatics
[c]Neuroscience Research Institute
[d]Department of Molecular, Cellular and Developmental Biology
University of California, Santa Barbara, CA 93106, USA

Abstract

Purpose: To develop an automated nuclei detection tool that provides reliable and consistently accurate results for counting cell nuclei.
Methods: We propose a simple yet robust method to analyze large sets of digital micrographs. The nuclei detector design is based on a Laplacian of Gaussian filter. We use the leave-one-out cross validation method for estimating the generalization error, which is then used to choose the model and parameters of the proposed nuclei detector with both fluorescent and dye stained images. We also evaluate the performance of a nuclei detector by comparing the results with manual counts.
Results: When our nuclei detector is applied to previously unseen images of feline retina, it correctly counts nuclei with an average error of 3.67%. Our approach accurately identifies the location of cell bodies. We also test the proposed method with various images and show that it is applicable to a wide range of image types with nuclei varying in size and staining intensity. The nuclei detector is developed as an ImageJ plugin and currently available at UCSB's Center for Bio-image Informatics website (http://www.bioimage.ucsb.edu/software.html).
Conclusions: The proposed method is simple and reliable. It also has widespread applicability to a variety of sample preparation and imaging methods. Our approach will be immediately useful in quantifying the number of cells in large sets of digital micrographs and from high-throughput imaging.

1 Introduction

Cell addition and loss are important biological events in development and pathology. As a result, counts of cells and nuclei from histological sections provide quantitative information central to studying changes in cells, tissues, and organs. For example, neuron number is a fundamental determinant of brain function (Williams and Rakic [1988]) and the number of photoreceptors is a common measurement of visual function of retina (Paskowitz et al. [2004], Michon et al. [1991], Lewis et al. [2002], Sakai et al. [2003], Fisher et al. [2005]). While progress in understanding changes in such parameters as cell structure or protein expression has been rapid during the past few decades, methods for determining cell number have remained limited. Determining the numerical density of cells in sectioned materials is difficult. Indeed, even the most rigorous studies rarely claim precision greater than $\pm 10\%$ (Williams and Rakic [1988]). Consequently, only marked changes or effects can be analyzed with confidence. Several solutions to this problem have been proposed, but they require significant resources in order to complete a morphometric analysis. Moreover, most of these methods still require manual counting, which is tedious and time consuming, regardless of whether a 2-D or a 3-D methodology is employed. In carrying out such work, biologists need to sit for long periods of time performing microscopic sampling and such physical and mental fatigue can impact the speed and quality of information. Problems that demand greater accuracy and reliability cannot be resolved with current manual methods.

Image analysis methods have been developed for nucleus detection or segmentation. In the past, algorithms developed for automatic micrograph analysis have been very task specific and are not easily extensible to analysis of different types of images such as those generated by immunofluorescence. For example, Malpica (Malpica et al. [1997]) used watershed to segment clustered nuclei, Roysam (Lin et al. [2005]) used watershed with recursive tree-based algorithm to segment nuclei in the rat hippocampus, Nedzved (Nedzved et al. [2000]) used morphological operators to segment cells in images with sparse density, Demandolx (Demandolx and Davoust [2001]) used a gray level thresholding method to segment subcellular structures in Hela cells and Sjostrom (Sjostrom et al. [1999]) used artificial neural network (ANN) to automatically count cells. Additionally, there is some commercial software that provide object-counting and feature detection (MetaMorph [2005], BioQuant [2006]). However, these tools often fail to provide reliable results and require intensive user interaction in order to obtain user-given initialization or parameter settings for accurate results. This often discourages biologists from using them. Additionally, these tools were not designed to analyze immunofluorescent retinal images, which present unique challenges, especially in tissue like the retina where cells are densely packed (600 cells in 512 x 100 pixels), uneven staining can cause intensity variations within cell layers, and non-uniform DNA distribution inside the nucleus can cause intensity variations within individual cells. Therefore, there is a need to develop a new method for automatically counting nuclei with consistently high accuracy and reliability in large sets of digital micrographs.

In this paper, we present methodology for *automatically* detecting nuclei, and therefore cell bodies, from a 2-D digital micrograph. The proposed approach provides an accurate, simple, and reliable method to count cells, nuclei, or other objects in sectioned materials. In order to have a scientific basis for selecting optimal parameters of the method, we mainly focus on retinal images, and here on the outer nuclear layer (ONL). Specifically we detect fluorescent photoreceptor nuclei from confocal images of control and degenerating feline retina as a result of retinal detachment. To show that the proposed method can be applied to many types of images without significant effort, we also tested it with images acquired by transmitted light and epi-fluorescent microscopy. The proposed nuclei detector has a number of advantages over manual analysis and other currently available or proposed automatic/semi-automatic methods including objectivity, simplicity and applicability.

2 Methods

2.1 Materials

The basis of our study is a set of immunofluorescence retinal images which have been collected by confocal imaging for understanding the mechanism underlying the loss and recovery of vision following retinal detachment/reattachment. Photoreceptor cells have received the greatest attention in these studies since photoreceptor outer segment degeneration and cell death are considered the primary effect of detachment. Previously it has been shown that the number of photoreceptors decrease after detachment (Anderson et al. [1983], Lewis et al. [2002]) (See Figure 1). Such degeneration of photoreceptors has been measured in various ways in different studies (Li et al. [1985], Lewis et al. [2002], Michon et al. [1991]): (1) the number of rows of nuclei in the outer nuclear layer (ONL), (2) area, (3) the thickness of the ONL, and (4) the number of nuclei. The values of these measurements are usually represented as change over time and then used as an index of photoreceptor degeneration. It has been verified that the ONL appears to be much more loosely packed with nuclei than normal as a result of loss of cells following detachment (Lewis et al. [2002], Fisher et al. [2005]). The ONL thickness or area may not always give an accurate measure of cell loss. We therefore used these data to compare with results obtained using the newly developed automated nuclei detector.

The retinal images used for cell counting were acquired from UCSB's Center for Bio-image informatics database (http://www.bioimage.ucsb.edu). The preparation of the retinas including the detachment procedure, fixation and sectioning of tissue has been published previously (Lewis et al. [2002]). The nuclear stain TOPRO (1:1000; Molecular Probes, Eugene OR) was added to 100 μm thick vibratome sections for 2 hr. After rinsing in phosphate buffer, the sections were mounted on glass slides using n-propyl gallate in glycerol and viewed on an Olympus FluoView confocal microscope.

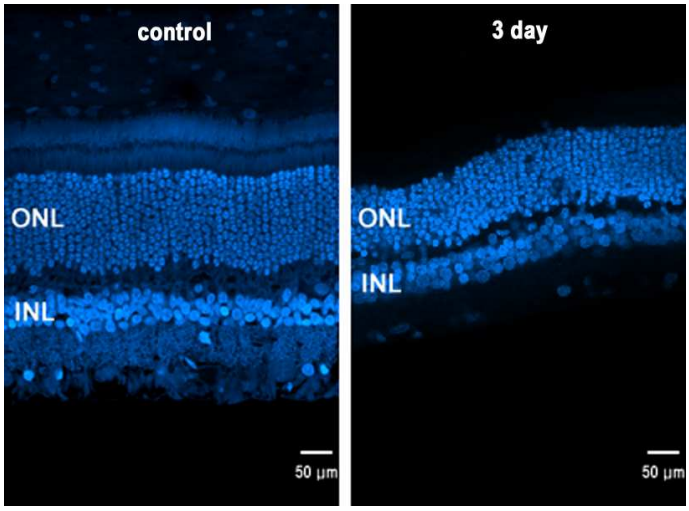

Figure 1: Photoreceptor death during retinal detachment. Confocal images of normal and detached retinas stained with the nucleus dye, TOPRO. After a 3 day detachment, the ONL appears to be thinner than the control attached tissue.

2.2 Nuclear modeling

Filtering is a very general technique of transforming image gray levels so as to enhance certain features of interest. Template matching is a simple filtering method for detecting a particular feature in an image. If the appearance of this feature in the image is known accurately, one can try to detect it with a corresponding template. This template is a subimage that looks just like the image of the object. A similarity measure is computed which reflects how well the image data match the template for each possible location.

Figure 2 shows a confocal image of normal feline retina illustrating the nuclear layers of the retina. In the image, nuclei can be approximated as simple, nearly circular shapes, which we will call *blobs*.

An image of nuclei usually shows a slice of the nuclei. The boundary of each nucleus shows up as strong intensity discontinuities in an image and the intensity distribution of some nuclei are multi-modal because of inconsistent staining and biological characteristics such as the DNA distribution (Figure 3 (a) and (b)). However, the intensity distribution can be assumed to be uni-modal under the appropriate amount of Gaussian blurring. After Gaussian blurring, the profile of a nucleus becomes a ridge with smooth change of gray level. Therefore, a *blob* can be modeled as a 3-D surface generated by rotating a ridge profile around its central axis (Figure 3 (c)). If we model the nuclei as this blob with some additive Gaussian noise, we can design an optimum linear blob detector by rotating the second derivative of a Gaussian around its central axis.

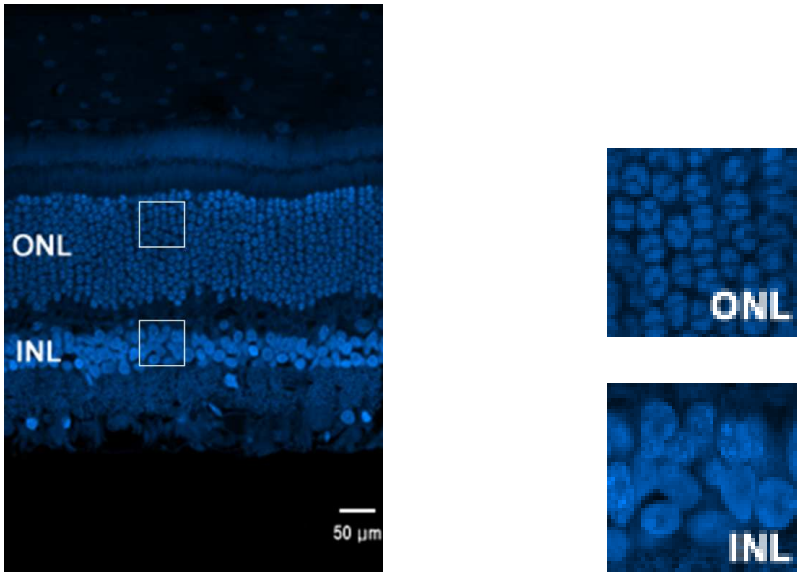

(a) (b)

Figure 2: Observation of nuclei in a confocal image of normal retina. Each nucleus can be approximated as a circular object, a blob. (a) Example confocal image of normal feline retina stained by TOPRO illustrating the nuclear layers. (b) Higher magnification images of regions of the outer nuclear layer (ONL) and the inner nuclear layer (INL). Such intensity variation is associated with the DNA distribution within these cells.

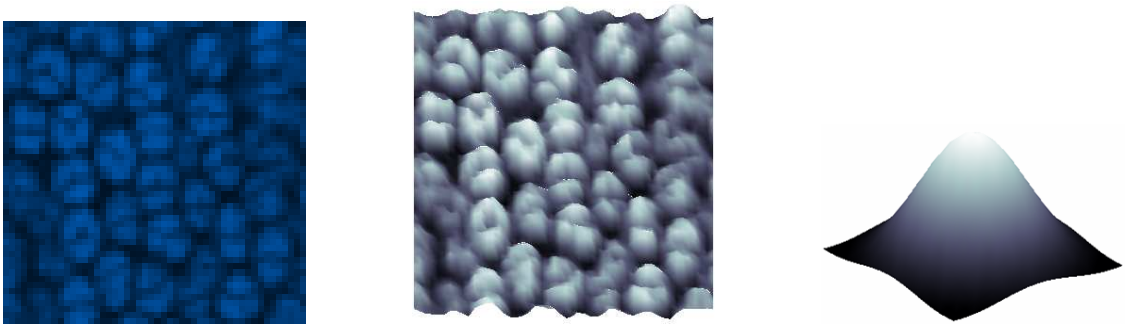

(a) (b) (c)

Figure 3: Nuclear modeling. (a) Example image of the outer nuclear layer within a feline retina stained by TOPRO. (b) 3-D surface plot of (a): the height of each point on the 3-D surface corresponds to the intensity of each pixel in the image (a). Each nucleus is represented by multiple peaks caused by variation of DNA distribution within a cell, however, it can be modeled as a unimodal intensity distribution shown in (c). The model is used as a template to detect cells in an image.

In our work, we utilize the inverted Laplacian of Gaussian (LoG) as our blob detector. We model the nuclei as circular objects although these objects mostly resemble ellipsoids. Our object in using a circular model, a very general shape model, is to achieve a rotation invariance in our detection. Otherwise it is possible that we are overfitting our design to the training images.

2.3 Nuclei detector design

Once we have a blob detector, the blob centers are detected with the following two steps:

1. **Blob detector design.** The LoG filter is designed such that the diameter of the filter is proportional to the average diameter of nuclei in the image. For example, the average size of cell bodies in the feline retina is 4-6 μm so the diameter of the filter can be set as 5 μm. The filter size in μm can be easily converted to pixel size by using the metadata embedded in a given image. The given retinal image is then filtered by the LoG. This operation results in a smooth continuous image of which the local maxima correspond to blob centers.

2. **Search for local maxima.** We search the filtered output for local maxima. The minimum distance between blob centers is used as the search radius for the local maxima, and this parameter is defined to be proportional to the filter size.

A schematic diagram for a nuclei detector is shown in Figure 4.

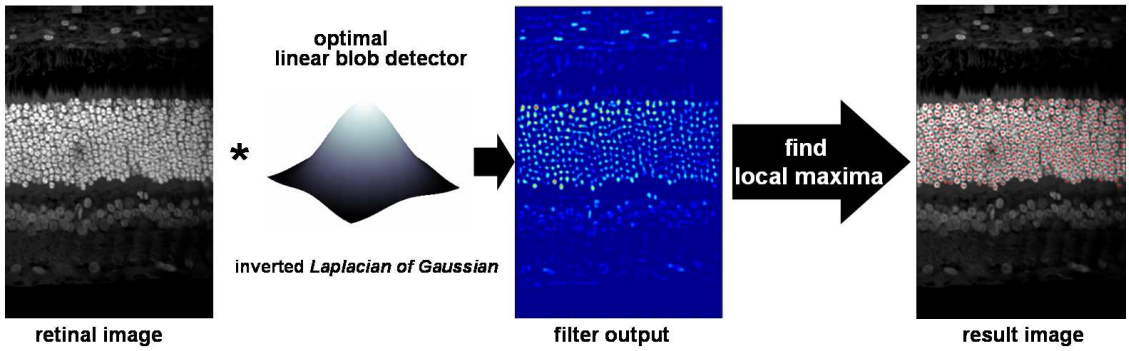

(a)

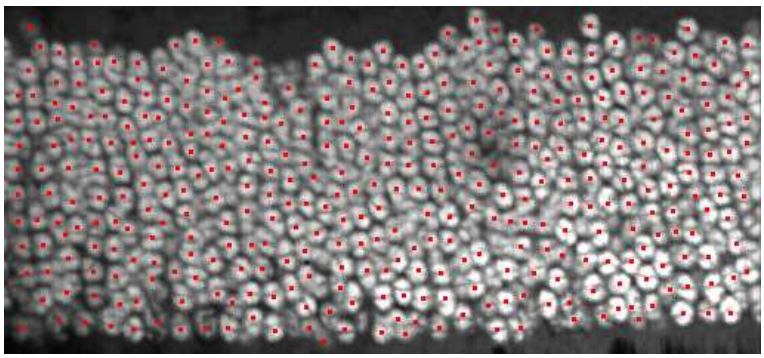

(b)

Figure 4: Nuclei detector design. (a) Schematic diagram of the nuclei detector: the blob centers are detected by filtering with the blob detector followed by searching local maxima. (b) Higher magnification of the outer nuclear layer within the result image in (a)

2.4 Evaluation of the nuclei detector

The goal of the nuclei detector is to generate counts of nuclei within the tissue layer of interest that are close to that obtained by manual counting. The manual count value, which is known as ground truth, is compared with the results of the automatic nuclei detector using various combinations of parameters. To estimate optimal parameters of the nuclei detector, we evaluate its performance using error criterion as

$$E \triangleq \frac{1}{N} \times \frac{|ND - GT|}{GT}, \tag{1}$$

where N is the number of images in the training set, ND and GT is the number of nuclei detected by our nuclei detector and by manual counting, respectively.

Because manual counting is time-consuming, we obtained ground truth for only 41 retinal images and, due to our small data set, we employ the leave-one-out cross-validation method to evaluate the detector's performance. That is, we train the nuclei detector 41 times, each time leaving out one image from the training data set, and using only the omitted image to compute the error. The resulting estimates of generalized error are used for choosing the optimal parameters for the nuclei detector.

Because the proposed nuclei detector uses a LoG filter and searches the local maxima of the filter output, its performance depends on two factors. First, how well the filter approximates the shape of a nucleus which is in turn determined by filter size and standard deviation σ. Second, how well the local maxima are determined, which is dependent on the minimum distance between blob centers. Since we search the filter output for local maxima, σ does not affect the performance of the nuclei detector. Thus, we vary two parameters: cell size (cs) in μm and the proportion (p) of the minimum distance between blob centers and filter size (fs), where fs is defined as $cs\times$ pixel resolution of a given image. The parameter cs is varied by five different values from 4 to 8. The range of the values is determined by the cell size within the Outer nuclear layer (ONL). The parameter p varies by ten different values from 0.1 to 1. Thus, we have a total 5×10 combinations, and 41 runs are conducted for each combination. We find the nuclei detector achieved a maximum performance at $cs = 5\mu m$, $p = 0.5$. Users simply can apply the optimal parameters to any type of retinal images without additional training. The summary of test result is shown in Figure 5.

3 Results

The present work is motivated by the development of an automatic detection solution for blob-like structures in various bio-molecular images. In such contexts, a nuclei detector requiring minimal user interaction is preferred. For this reason, a proposed nuclei detector should be 1) accurate so that it can approximate manual counting; 2) simple and computationally efficient: providing reliable results; 3) applicable to a wide variety of image types with minimal user interaction including

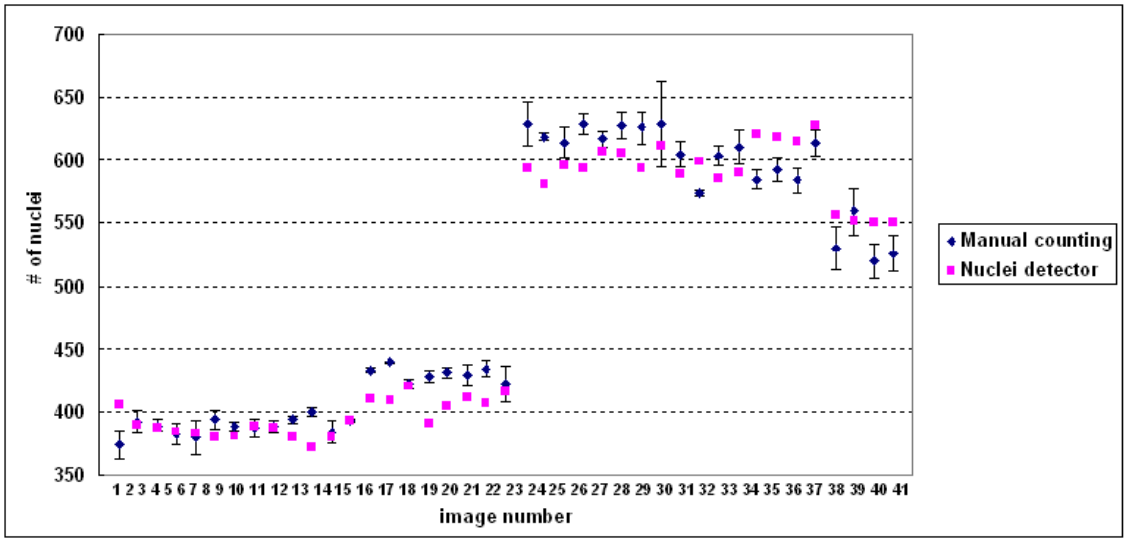

Figure 5: A summary of test results of 41 images. Blue dots denote manual counting and the error bar of each blue dot indicates intra-observer variation. Pink dots represent the result of the automated nuclei detector. The nuclei detector does not systematically overestimate or underestimate the number of nuclei compared to the manual counts.

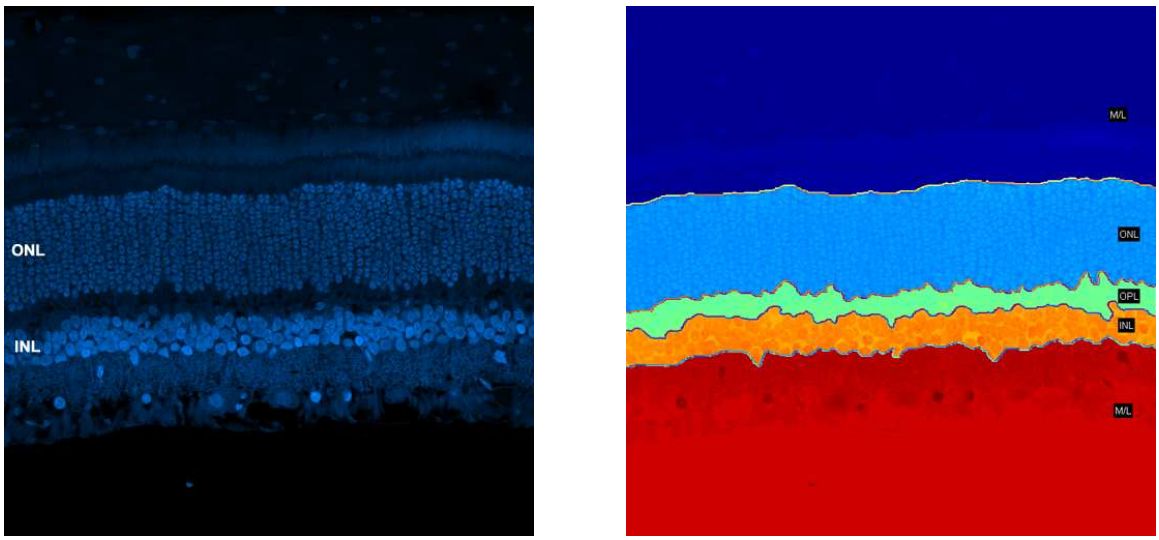

(a) (b)

Figure 6: Example image of a layer map created from a retinal image. (a) Confocal image of a normal cat retina stained by TOPRO. (b)Layer map of (a). Boundaries of layers are outlined manually by using a tablet PC.

parameter settings or preprocessing of the given image. To show that our nuclei detector satisfies these three issues, we applied it to various sets of retinal images (e.g. confocal images of cat retina and transmitted light microscope images of mouse retina) as well as other images commonly generated by biologists (e.g. DNA dot blots and fluorescent cell images).

3.1 Accuracy

Application to confocal images of the retina. We presented the results of applying the nuclei detector to a series of confocal images of control and detached retinas. Here we focused on detecting nuclei within the outer nuclear layer (ONL) and the inner nuclear layer (INL). 41 digital images of normal and 3-day detached feline retinas (21 control images and 20 3-day detached retinal images) were generated with an Olympus FluoView laser scanning confocal microscope from tissue sections stained with TOPRO. For each image, we manually created a mask to define the boundary of the ONL and the INL by using a tablet PC (Figure 6). We created a data collection of the extracted region of the ONL and the INL with corresponding masks for all images. The same collection was used for manual counting to create ground truth. For the ONL, each image was manually counted three times independently to measure intra-observer variation. The average variation over 41 images was 1.8 % ranging from 0.2 to 5.35 %.

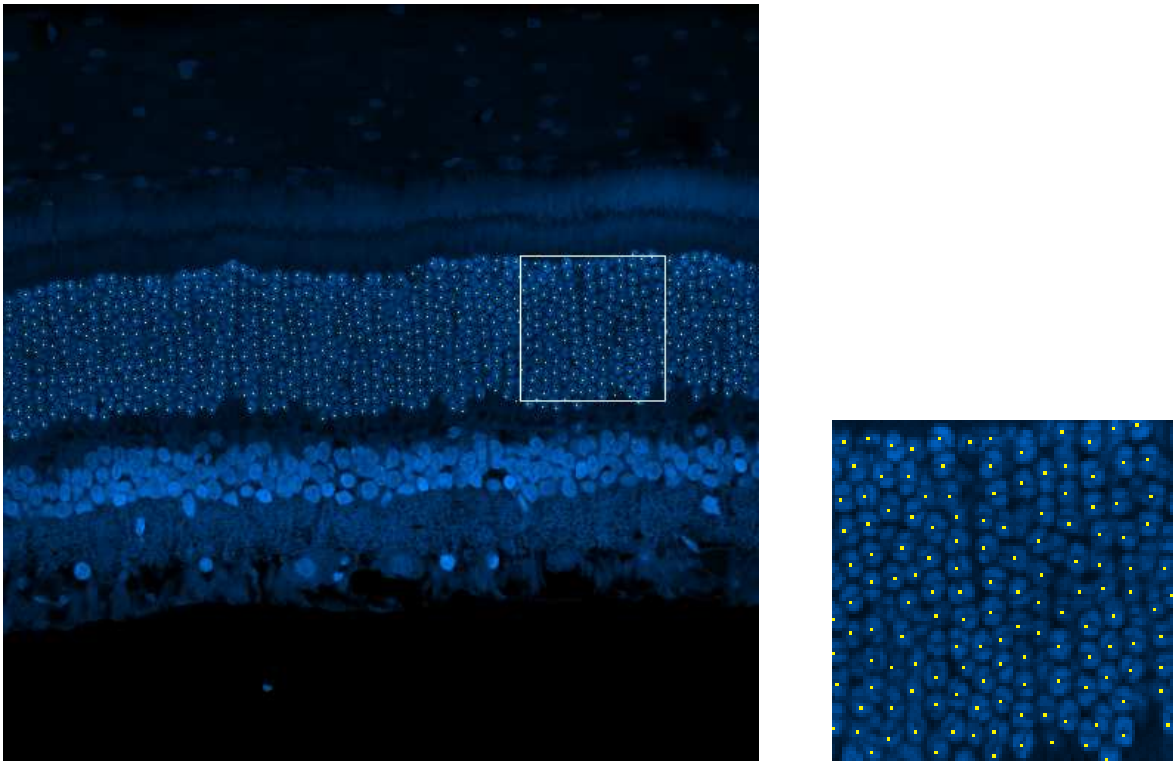

(a) (b)

Figure 7: Application of the nuclei detector to a retinal image. (a) Confocal image of a normal cat retina stained by TOPRO. Detected cell centers are marked with yellow points. (b)Higher magnification of the part of the image in (a) denoted by the white rectangle. 688 cells are detected with 0.5% error compared with manual counts (690 cells).

.

We estimated optimal parameters for the nuclei detector through the leave-one-out cross validation described in Section 2.4. Then we applied the optimized nuclei detector to the data set. To evaluate the performance of the nuclei detector, the result was compared with the ground truth. The automated nuclei detector approximated the number determined by manual counting. The average absolute error of the nuclei detector was 3.67% for the ONL and 8.52% for the INL respectively. Considering intra-observer variation is 1.8%, the results from our nuclei detector was promising. Even though we did not have a ground truth of (x,y) coordinates of detected nuclei, the location of detected nuclei overlayed on the image seemed visually acceptable (See Figure 7 and 8). Note that the contrast of the image shown in Figure 8 was not high enough to assure visibility so that variation among the three manual counting results of a given image became relatively high at 3.37%

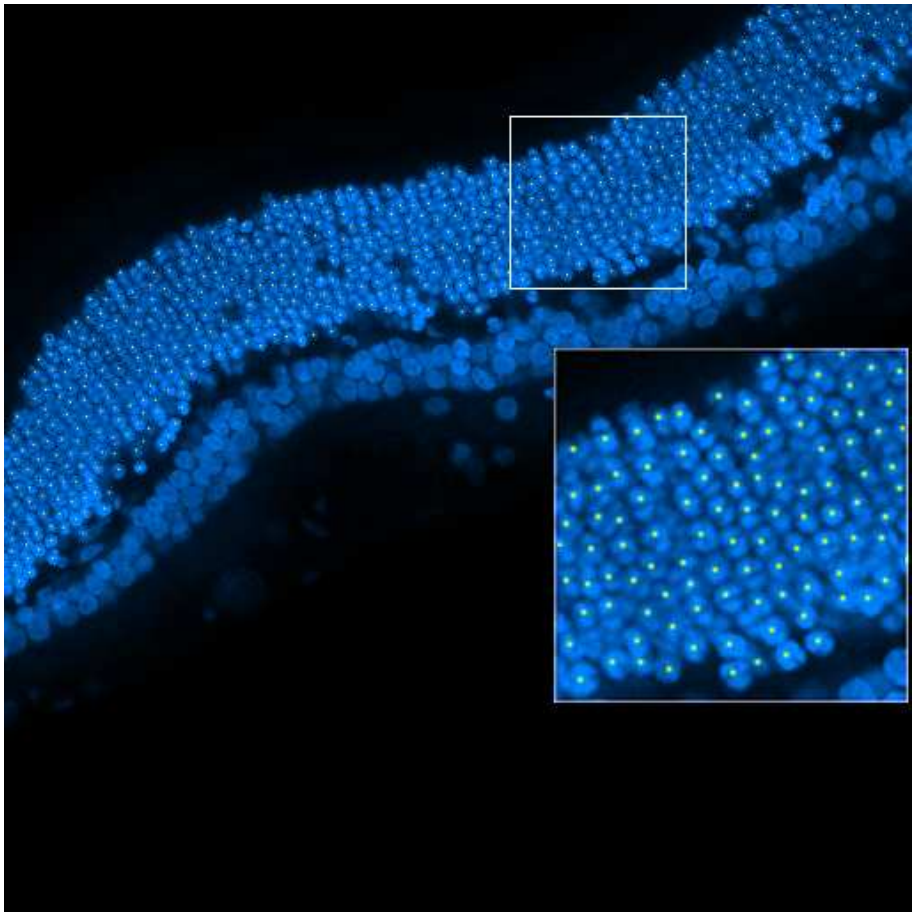

Figure 8: Application of the nuclei detector to a difficult case: applying the nuclei detector to a diagonally oriented confocal image of a 3-day detached cat retina stained by TOPRO. The image was acquired with poor contrast. Detected cell centers are marked with yellow points. 606 cells are detected with 3.5% error compared with manual counts (628 cells).

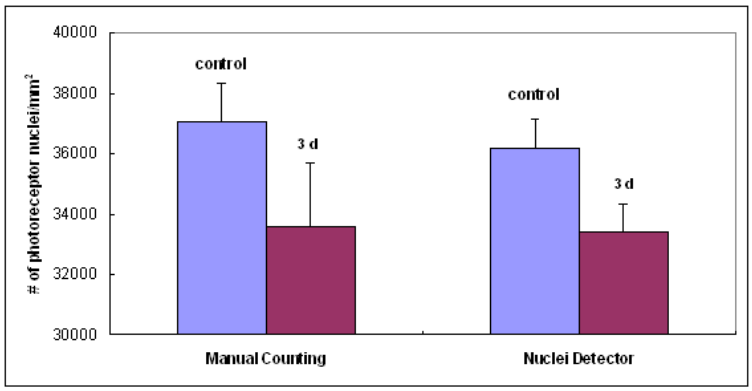

Figure 9: A comparison of manual and nuclei detector counts of the average number photoreceptor nuclei per mm^2 of retina in control and 3 day detached retina. (a)Manual counts. The control retina had, on average, 37503 nuclei/mm^2. After 3 day of detachment, the cell count was reduced to an average 33590 nuclei/mm^2 (p=0.0001). (b)Nuclei detector counts. The control retina had, on average, 36164 nuclei/mm^2. After 3 days of detachment, the cell count was reduced to an average 33417 nuclei/mm^2 (p=0.0000007).

Applying cell counting to retinal detachment. The cell count was used to verify the finding that the number of photoreceptors decrease in response to a retinal detachment. In the feline model, retinal detachment leads to the death of some photoreceptor cells (Lewis et al. [2002], Fisher et al. [2005]). Figure 9 shows the average number of photoreceptor nuclei per mm^2 of retina in control eyes and those with 3-day detached retinas using the manual counting method. The control retina have, on average, 37503 nuclei/mm^2. After 3 days of detachment, this number is reduced to an average of 33590 nuclei/mm^2 (p=0.0001). Even though the average number of photoreceptor nuclei is not exactly the same as the manual count, the nuclei detector captures relative differences in cell density between normal and 3-day detached cases and reaches the same conclusion as manual counting (Figure 9). For the INL, manual counts in 3-day detached retinas would not be considered statistically different from those in normal retinas (p=0.05309 $>$ 0.05) (Figure 10). Thus, both manual counting and the nuclei detector result in the same conclusion; *the number of cells within the INL does not change in response to retinal detachment.* To date cell death in the INL after detachment has not been reported for this species.

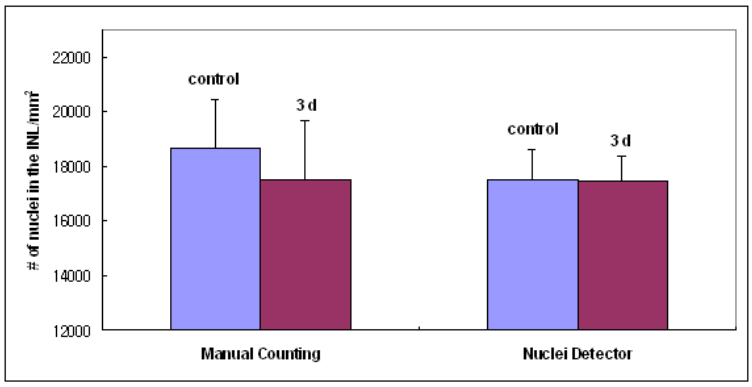

Figure 10: The average number of nuclei within the INL per mm^2 of retina in control and 3 day detached retina. (a)The graph is created from manual counts. The control retina have, on average, 18659 nuclei/mm^2. After 3 days of detachment, the cell count is reduced to an average 17516 nuclei/mm^2 ($p=0.05309 > 0.05$). (b)The graph is created from results of the nuclei detector. The control retina have, on average, 17501 nuclei/mm^2. After 3 days of detachment, the cell count is reduced to an average 17435 nuclei/mm^2 ($p=0.9755 > 0.05$).

Application to large field of view images. We applied the nuclei detector to a mosaic consisting of eight overlapping images of 3 day detached cat retina (Figure 11 (a)). These images were acquired with 5 to 20% overlap in order to align multiple images automatically. To ensure high quality results containing the maximum amount of original unchanged data blended without blur and abrupt intensity differences, a modern blending technique was used (Fedorov et al. [2002]). By using a mosaic, we can count photoreceptor nuclei within a large section of the cat retina without sampling the tissue. There had previously been a large amount of work to estimate cell numbers from the average cell density of the region in which counting boxes are distributed (Abercrombie [1946], Howard et al. [1985], Williams and Rakic [1988]). From this work, it has been determined that the larger the tissue and steeper the gradients in cell density, the greater the margin of error. The proposed nuclei detector overcame these potential errors because no assumptions were made about size, shape or regional difference in cell density. Therefore, it provided not only reliable results with greater confidence but also greater insight into relationships between cells and tissues.

3.2 Applicability to varying sample preparation

Application to laser scanning confocal images stained with antibodies. We applied our method to confocal images stained with various antibodies. In particular, images were used where the antibodies did not identify the nuclei above background levels and the primary purpose of the images was not to produce information about cell nuclei. Since confocal retinal images are generated by using fluorescence, only specific regions where fluorescent dye molecules are bound are visualized. Therefore, the brightness range within the image is very small. If the antibody does not bind to the ONL, then the ONL usually appears as a dark region where the intensity value of a pixel is close to zero (Figure 12 (a)). The histogram shown next to the image is a plot of number of pixels at each of the 256 possible brightness levels. The narrow peak indicates that only a few of the levels are represented. Since the brightness range within the image is very small, there is not enough contrast to visualize the structure within the ONL. Therefore, the visibility of the ONL should be improved by stretching contrast so that the value of pixels are reassigned to cover the entire available range thus making the nuclei visible. We applied a histogram equalization method (Russ [1995]) to the image so that individual nuclei within the ONL could be discriminated (Figure 12 (b)). This histogram plotted with the image in the Figure 12 (b) now shows counts of pixels for gray levels that are spread out across the available brightness scale (Figure 13). The results showed that the proposed method estimate the location of a cell body even though the antibody used is not traditionally thought of recognizing and binding to nuclear portions of the cell. In this context, cell counting does not need to be limited to stains such as TOPRO or DAPI. Furthermore, our nuclei detector performed better than manual counting especially where the the contrast of the region is low (Figure 13 (e) and (f)). Since our approach estimates local maxima of the filter output, the nuclei detector still can identify individual nuclei even if the contrast of the region is low or the intensity within the region varies dramatically.

(a)

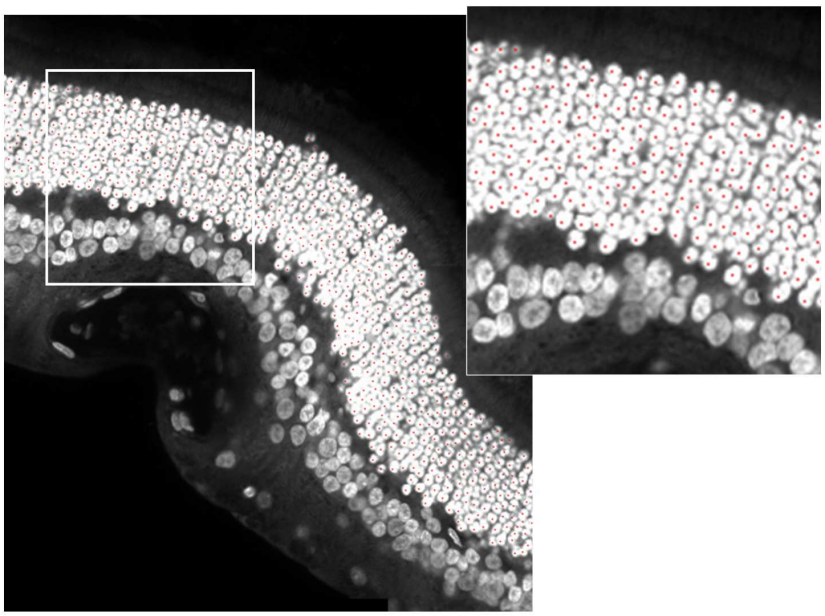

(b)

Figure 11: Application to large images. (a)A 2.8 mega pixel montage automatically assembled using eight confocal images of 3 day detached cat retinas stained with TOPRO. Detected cell centers are marked with red dots. A portion of image (a; boxed) is displayed at higher magnification and subsequently the boxed area in (b) is shown at higher magnification.

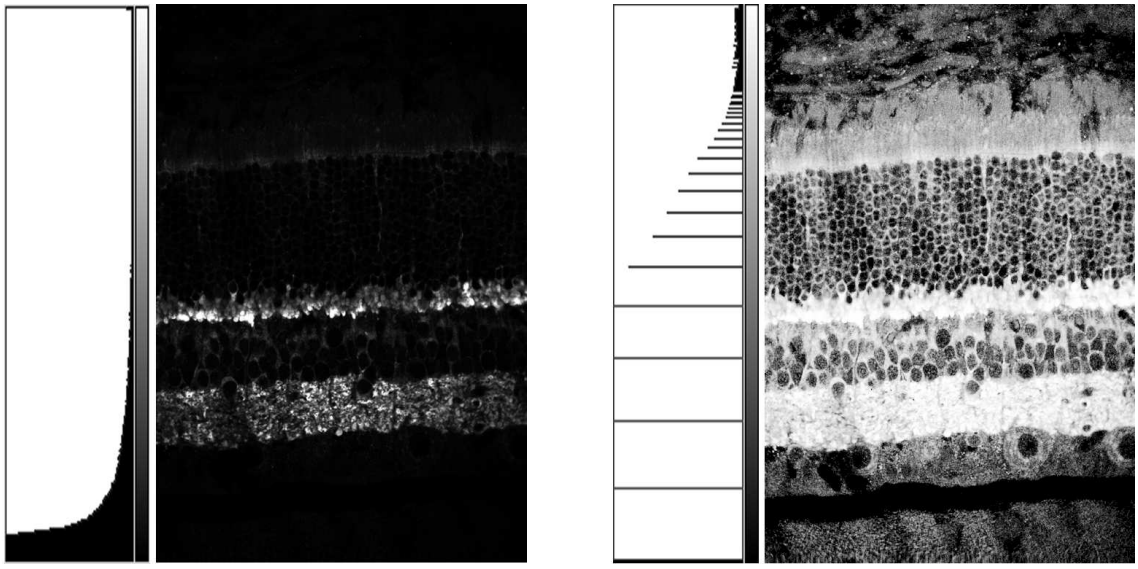

(a) (b)

Figure 12: Example image of contrast enhancement by a histogram equalization. (a) Example of single antibody labeled image of synaptic terminals labeled with anti-synaptophysin. (b) Histogram equalized image shows a full range of black to white values.

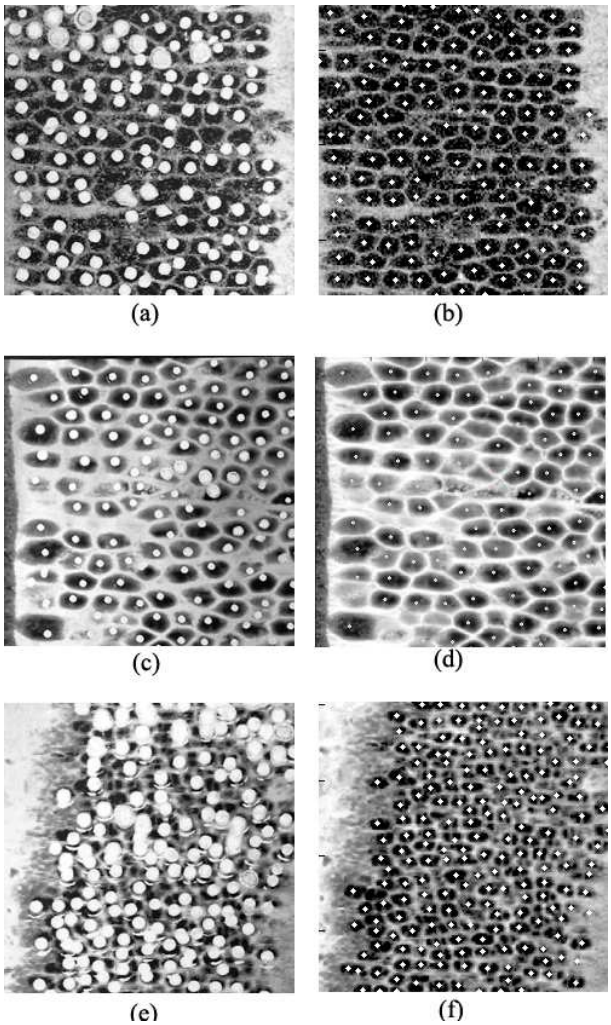

Figure 13: A comparison of images manually counted and counted with the nuclei detector. (a),(c) and (e) Manually counted images. The nuclei were counted on the printed paper by placing dots over the nuclei. The paper was scanned to create a digital image. (b),(d) and (f) Nuclei detector. White dots on the image represent detected nuclei.

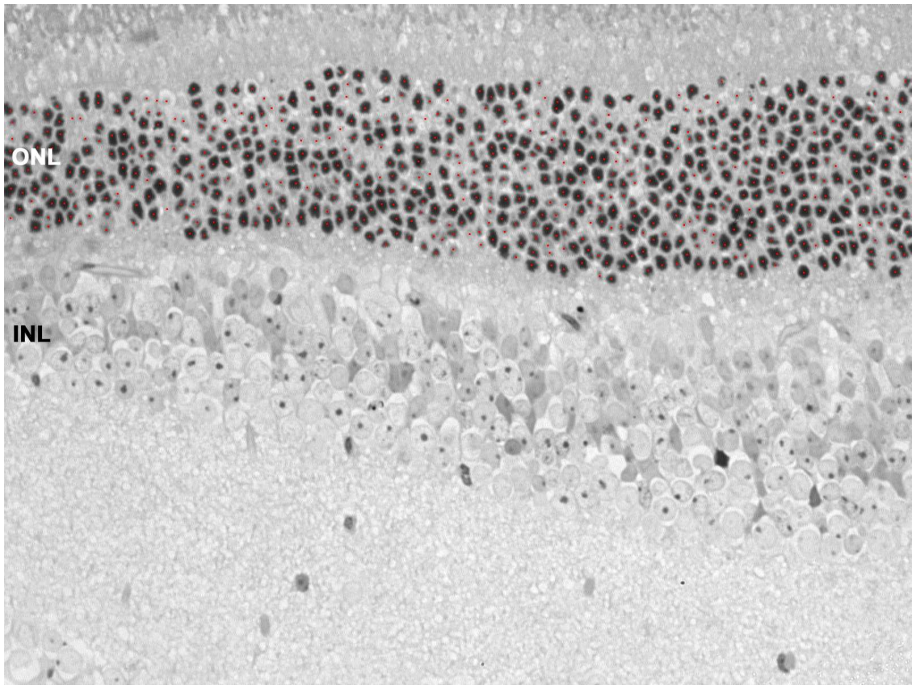

Figure 14: Light micrograph of normal mouse retina. The tissue was embedded in resin sectioned at 1 μm and stained with Toluidine blue.

Application to bright-field images of retina. We also applied the nuclei detector to images generated by transmitted light microscopy of normal mouse retina (Figure 14). The filter size was set to 30 pixels and the minimum distance between blob centers was set to 15 pixels (filter size $\times$ 0.5), which was the same optimal parameter calculated from feline retina. The result showed that the proposed method can approximate the center of a cell very well even without fine tuning of parameters.

Application to other images. We tested the proposed method with various images without tuning parameters. Figure 15 (a) shows an image of cultured cells and demonstrate that nuclei can be detected with a single filter even though the size of nuclei within the image are all different. Similarly, Figure 15 (b) consists of various shapes and sizes of blobs. By applying a single filter with a median size of blob within an image, we could detect all blobs successfully. There were double detected blobs because their sizes were almost twice as big as the others, however, they can be easily post processed by a simple morphological operation. Estimating local maxima can detect some false positive blobs, but they could also be eliminated by tuning the parameters. Additionally, the nuclei detector still could identify the individual dot even when the image was noisy (See Figure

15 (c)).

3.3 Practicality

A number of manual counting methods have been developed. While they are accurate, they are often difficult and tedious to use. The proposed nuclei detector is a simple and automated method. However, a filter size and the minimum distance between cells must be defined. The default value of the minimum distance can be set as half of the filter size as was shown before (Section 2.4) and the filter size can be selected roughly from a given sample image. In biological fields, the information of cells including cell size is usually well known. Therefore, the added effort is not significant.

4 Discussion

In this paper, we designed a nuclei detector which automatically detects the number of nuclei in digital micrographs and can thus be used for counting cells. Initially, we evaluated the performance of the nuclei detector over confocal images of feline retina but found it useful for a wide variety of preparations. The proposed nuclei detector performed very well with an average error of 3.67%. The advantages of the proposed method are simplicity and reliability to detect any blob-like structures such as cells. For example, when using this method to detect cells in retinal tissues, no parameters need to be set. Moreover, it is computationally efficient so it is applicable to whole tissue instead of tiling part of the region of interest within a tissue. This eliminates the potential error caused by tissue sampling. It is especially valuable for tissue with a steep gradient in cell number such as brain and retina. Additionally, the proposed method can be used on a variety of preparations or imaging methods, indicating its widespread applicability.

We used a histogram equalization to enhance the visibility of an image. The histogram equalization method increases the visual contrast for the pixels present, but it does not increase the ability to discriminate subtle variations in gray scale that are not in the original image. It also magnifies the brightness difference associated with noise in the original image. Therefore, we need to develop a new contrast stretching method so that we can increase the contrast while suppressing the brightness of noise.

Automated measurement on microscope images is becoming an increasingly important tool in biology. The technique we suggest here, for the automated detecting of nuclei is useful especially on a larger scale. Moreover, we can extract additional information based on nuclei detection result including thickness of a layer and the local cell density within the region (e.g. a specific layer of the retina or brain) (Byun et al. [2006]). We found that quantitative analysis based on nuclei detection not only corroborated conclusions derived from manual measurements and qualitative assessment, but also provided significant information about local structural changes during retinal detachment. This additional information will help to answer the questions such as is thickness of

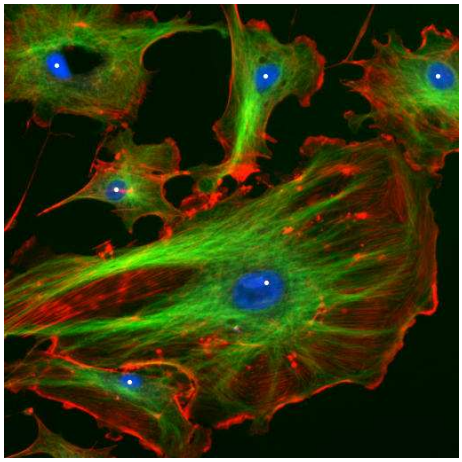

(a)

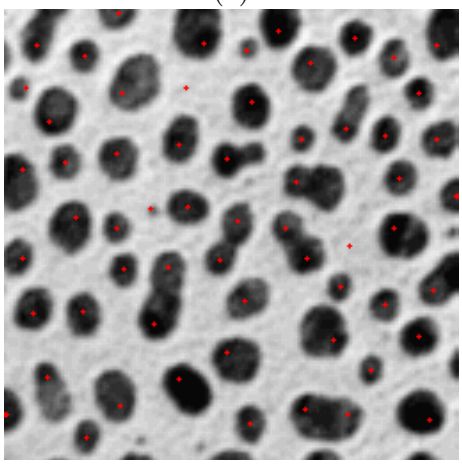

(b)

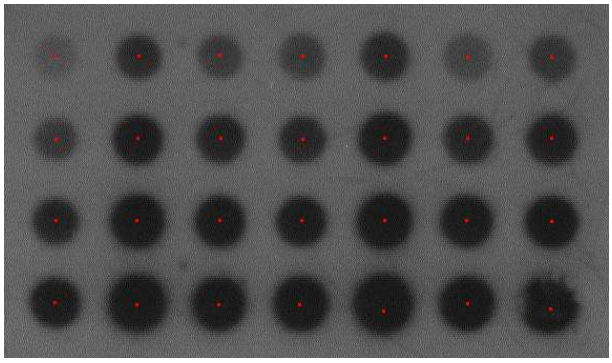

(c)

Figure 15: Application of the nuclei detector to different types of images. (a)A fluorescent cell image acquired by an epi-fluorescent microscope: actin (red), β-tubulin (green) and nuclei (blue) (downloaded from ImageJ [2005]). Six nuclei are detected. (b) Blob image (downloaded from ImageJ [2005]). 61 blobs were detected with four detected twice and three false positive blobs. (c) DNA dot blots (downloaded from ImageJ [2005]). All 28 dots were detected.

the ONL correlated to the density of cells? Is it possible to discriminate cone from rod by looking at DNA distribution within a nucleus?

The proposed nuclei detector has been implemented as a plug-in for the public domain NIH image processing and analysis program, ImageJ (v.1.34 developed at the US National Institutes of Health and available at http://rsb.info.nih.gov/ij/index.html). Nuclei detector with sample images and its instruction is available at http://www.bioimage.ucsb.edu/software.html.

5 Acknowledgements

We wish to acknowledge Camille Cazon for manual counting, Kellen Betts for the sample preparation, Thomas Kuo for developing the ImageJ plug-in and Dmitry Fedorov for providing the mosaic images. This research is supported by NSF #ITR-0331697 and NIH # EY-00888.

References

M. Abercrombie. Estimation of nuclear population from microtome sections. *The Anatomical Record*, 94:239–247, 1946.

D. Anderson, W. Stern, S. Fisher, P. Erickson, and G. Borgula. Retinal detachment in the cat: the pigment epithelial-photoreceptor interface. *Invest Ophthalmol Vision Science*, 24:906–926, 1983.

BioQuant. BioQuant: Image analysis corporation, 2006. http://www.bioquant.com/ [visited Feb 2nd, 2006].

J. Byun, N. Vu, B. Sumengen, and B. S. Manjunath. Quantitative Analysis of Immunofluorescent Retinal Images. In *IEEE International Symposium on Biomedical Imaging: From Nano to Macro (ISBI)*, Arlington, Virginia, USA, April 2006.

D. Demandolx and J. Davoust. Multiparameter image cytometry: from confocal micrographs to major subcellular structures in fluorescence microscope images of hela cells. *Bioinformatics.*, 17 (12):1213–1223, 2001.

D. Fedorov, L. M. G. Fonseca, C. Kenney, and B. S. Manjunath. Automatic registration and mosaicking system for remotely sensed imagery. In *SPIE 9th International Symposium on Remote Sensing*, Sep 2002. URL `http://vision.ece.ucsb.edu/publications/02SPIEFedorov.pdf`.

S. K. Fisher, G. P. Lewis, K. A. Linberg, and M. R. Verardo. Cellular remodeling in mammalian retina: results from studies of experimental retinal detachment. *Progress in Retinal and Eye Research*, 24:395–431, 2005.

V. Howard, S. Reid, A. Daddeley, and A. Boyde. Unbiased estimation of particle density in the tandem scanning reflected light microscope. *Journal of Microscopy*, 138:203–212, 1985.

ImageJ. ImageJ:Image processing and analysis in Java, 2005. http://rsb.info.nih.gov/ij/images/ [visited Sep 18th, 2005].

G. P. Lewis, D. G. Charteris, C. S. Sethi, and S. K. Fisher. Animal models of retinal detachment and reattachment: identifying cellular events that may affect visual recovery. *Eye*, 16(4):375–387, 2002.

Z.Y. Li, M. O. Tso, H. M. Wang, and D. T. Organisciak. Amelioration of photic injury in rat retina by ascorbic acid. *Investigative Ophthalmology and Visual Sciences*, 26(1589), 1985.

G. Lin, M. Chawla, K. Olson, J. F. Guzowski, C. A. Barnes, and B. Roysam. Hierarchical, Model-based Merging of Multiple Fragments for Improved 3-d Segmentation of Nuclei. *Cytometry Part A*, 63A:20–33, 2005.

N. Malpica, C. O. de Solorzano, J. J. Vaquero, A. Santos, I. Vallcorba, J. M. Garcia-Sagredo, and F. del Pozo. Applying watershed algorithms to the segmentation of clustered nuclei. *Cytometry.*, 28(4):289–297, 1997.

MetaMorph. MetaMorph:the complete imaging solution, 2005. http://www.universal-imaging.com/products/metamorph/ [visited Jan 14th, 2005].

J. J. Michon, Z. Li, N. Shioura, R. J. Anderson, and M. O. M. Tso. A Comparative study of Methods of Photoreceptor Morphometry. *Investigative Ophthalmology and Visual Sciences*, 32 (2):280–284, 1991.

A. Nedzved, S. Ablameyko, and I. Pitas. Morphological segmentation of histology cell images. *ICPR*, 1:500–503, 2000.

D. M. Paskowitz, G. Nune, D. Yasumura, H. Yang, R. B. Bhisitkul, S. Sharma, M. T. Matthes, M. A. Zarbin, M. M. LaVail, and J. L. Duncan. BDNF Reduction of Retinal Toxicity of Verteporfin PDT. *Investigative Ophthalmology and Visual Science*, 45(11):4190–4196, 2004.

J. C. Russ. *The Image Processing Handbook*. CRC, 1995.

T. Sakai, J. B. Calderone, G. P. Lewis, K. A. Linberg, S. K. Fisher, and G. H. Jacobs. Cone photoreceptor recovery following experimental detachment and reattachment: an immunocyto-chemical, morphological, and electrophysiological study. *Investigative Ophthalmology and Visual Science*, 44:416–425, 2003.

P.J. Sjostrom, B.T. Frydel, and L.U. Whhlberg. Artificial nnerual network-aided image analysis system for cell counting. *Cytometry*, 36:18–26, 1999.

R. W. Williams and P. Rakic. Three-dimensional counting: An accurate and direct method to estimate numbers of cells in sectioned material. *Journal of Comparative Neurology*, 278:344–352, 1988.